International Forum on Aeroelasticity and Structural Dynamics
IFASD 2026
16-19 June 2026, Goettingen, Germany

AEROELASTIC MODEL UPDATE FOR A FLEXIBLE WING USING EXPERIMENTAL DATA

Gerrit Stavorinus[1], Pedro J. González[1], Guilherme C. Barbosa[1], Alvaro A. G. Quesada[1], Flavio J. Silvestre[1], Arne Voß[2], Wolf Krüger[2]

[1]Technical University of Berlin
Marchstraße 12, 10587 Berlin, Germany
g.stavorinus@tu-berlin.de
p.gonzalez.ramirez@tu-berlin.de
g.chaves.barbosa@tu-berlin.de
garcia.quesada@campus.tu-berlin.de
flavio.silvestre@tu-berlin.de

[2]DLR - German Aerospace Center
Institute of Aeroelasticity
Bunsenstraße 10, 37081 Göttingen, Germany
arne.voss@dlr.de, wolf.krueger@dlr.de

Keywords: Very flexible aircraft, model updating, wind tunnel testing.

Abstract: High-aspect-ratio wings improve aerodynamic efficiency but, due to their increased flexibility, introduce significant aeroelastic challenges, requiring accurate yet efficient modeling. Particularly with flexible, high-aspect-ratio wings, theoretical models can show large discrepancies in predicted loads and dynamic response compared to experimental results. This work presents a methodology for updating aeroelastic VLM/DLM models of highly flexible wings using experimental wing-root loads data acquired from wind-tunnel tests, thereby avoiding the need for detailed pressure measurements or high-fidelity CFD. The methodology uses an optimization routine to find the distribution of correction factors to alter the lift and moment distribution so that the error between measured and calculated wing root loads in static cases is minimized. The correction factors are applied to Nastran and Loads Kernel simulations. The updated model is validated by comparisons to static test cases and then applied to 1-cos dynamic wing root angle of attack and dynamic control surface deflection maneuvers. The updated model shows good agreement with the experimental results in both static and dynamic cases. The correction factors obtained using the methodology were applied to a model of a whole aircraft, showing a significant influence on static and dynamic behavior.

1 INTRODUCTION

The ambition to reduce the environmental impact of commercial aviation has driven interest in High Aspect Ratio Wings (HARW) aircraft as a way to increase the aerodynamic efficiency of aircraft and, therefore, reduce fuel consumption, which decreases both carbon emissions and operating costs. Maintaining structural weight while increasing the aspect ratio results in slender, more flexible wings with larger structural deflections and lower structural frequencies, leading to a growing interaction between structural dynamics, aerodynamics, and flight mechanics. Accurate prediction and modeling of these interactions is therefore essential to ensure flight safety and reliable performance assessments.

Aeroelastic models based on the finite element method (FEM) for structural dynamics, coupled with aerodynamic panel methods such as the Vortex Lattice Method (VLM) and Doublet Lattice Method (DLM), are widely used in aeroelastic analysis due to their computational efficiency and suitability for design iteration. These models inherently rely on simplifying assumptions like linearized potential flow, and as a result, discrepancies between numerical predictions and experimentally observed structural and aeroelastic behaviors are unavoidable. Higher-fidelity approaches, such as computational fluid dynamics (CFD)-based models, provide a more accurate representation of nonlinear aerodynamic effects, viscous phenomena, and flow separation. However, their significantly higher computational cost makes them impractical for preliminary design stages, rapid design iteration, or the simulation of a large number of dynamic maneuver cases. An effective compromise is the systematic updating of lower-cost aerodynamic panel models to improve their predictive capability while retaining computational efficiency. The goal of model updating is to reduce the error between numerical predictions and experimental observations (or higher-fidelity simulations) by calibrating model parameters or introducing correction terms. Panel methods already capture the dominant aerodynamic mechanisms governing aeroelastic behavior in the linear regime, and discrepancies that arise can be approximated through targeted corrections rather than fully resolved simulations. Early efforts in model updating focused on matching theoretical results with wind tunnel measurements, while later developments increasingly used CFD data as the reference. An assessment of model updating procedures was performed by Palacios et al. [1]. Giesing et al. proposed the Correction Factor Technique (CFT) to correct the results of DLM simulations in 1976 [2], which uses diagonal correction matrices to match experimentally measured quantities. The CFT differentiates between multiplicative pressure corrections and additive downwash corrections. The pressure correction can be expressed as

$$\mathbf{\Delta C_{p,exp}} = \mathbf{W_p} \cdot \mathbf{\Delta C_{p,theo}}. \tag{1}$$

with $\mathbf{\Delta C_{p,exp}}$ and $\mathbf{\Delta C_{p,theo}}$ being the vectors of pressure coefficients from experimental measurements and numerical simulation, respectively, and $\mathbf{W_p}$ being the diagonal matrix of correction factors to correct the theoretical pressure distribution. The model update now consists of finding an appropriate $\mathbf{W_p}$. Usually, this is an underdetermined system due to the much smaller number of experimental pressure measurement points compared to the number of aerodynamic boxes in the used panel methods. Giesing et al. handled this by using a Lagrange multiplier approach and least squares minimization, which minimized the difference between the initial numerical solution and the updated numerical solution while matching the measured pressures/pressure coefficients. The downwash correction to match the theoretical downwash $\mathbf{w_{theo}}$ to experimental values $\mathbf{w_{exp}}$ was presented initially in a similar form to the pressure correction however, Giesing et al. found that a downwash correction performed best when applied additively

$$\mathbf{w_{exp}} = \mathbf{w_{theo}} + \delta\mathbf{w}. \tag{2}$$

Many published correction techniques are based on this CFT method, with varying methods of obtaining the correction factor matrices [3–8]. Certain methods expand the technique to full matrices, introducing interference between boxes, which allows for the qualitative modification of the pressure distribution for example to induce a discontinuity at the location of a shock [4]. Modern aerodynamic model updating methods mostly rely on highly resolved CFD-based pressure data to calculate correction factors, making them inapplicable to cases in which CFD data is not available or validation against experimental measurements is desired. Particularly, wing root loads are typically not considered in aerodynamic updating methods or only considered in the form of integrated pressure data, although Giesing et al. already noted the advantages of including them in model updating. Accurate experimental pressure data can also be difficult to obtain for already constructed wings without considerable modifications, which might not be desirable. Thus, a method of correcting aeroelastic models of flexible aircraft in the absence of pressure information is necessary.

The Department of Flight Mechanics, Flight Control and Aeroelasticity of TU Berlin, in co-operation with the German Aerospace Center (DLR) Institute of Aeroelasticity, developed the TU-Flex flexible flying demonstrator [9,10]. The TU-Flex (shown in Fig. 1) is a flying aeroelastic testbed in a transport aircraft configuration with a modular design, permitting the gathering of flight mechanical and structural data for wing configurations with different levels of flexibility. The TU-Flex flexible wing (FW) is a high aspect ratio wing designed to exhibit wingtip deflections of around 10% during flight. The design process of the TU-Flex FW is detailed in [11]. Table 1 shows the main specifications of the TU-Flex FW.

Figure 1: TU-Flex during operational ground tests.

Table 1: General properties of the TU-Flex FW.

Property	TU-Flex FW
Span	1.8 m
Chord (root)	0.30 m
Chord (tip)	0.15 m
Taper ratio	0.5
Aspect ratio	16
Sweep	20°
Wing area	0.405 m^2
Mean chord	0.225 m
Airfoil	Eppler 214
Wing mass	2.2 kg

Static and dynamic wind tunnel tests were carried out with the TU-Flex FW demonstrator (shown in Fig. 2) at the Crosswind Simulation Facility (SWG) of the DLR Göttingen [12]. The TU-Flex FW provides a comprehensive experimental dataset and represents a relevant test case for the development of aeroelastic model updating techniques applicable to future flexible aircraft concepts.

Figure 2: TU-Flex FW in wind tunnel.

The objective of this paper is to describe a generally applicable methodology for obtaining correction factor matrices from experimentally obtained wing root loads data for use in Nastran and LoadsKernel [13, 14] static and dynamic aeroelastic simulations, using the TU-Flex FW as the sample case. Correction factor matrices that minimize the difference between experimentally measured and numerically calculated wing root shear force F_z, bending moment M_x, and torsion moment M_y are obtained for static cases at varying airspeeds, considering the wing root loads during different angles of attack. Since no constraints can be placed on the numerical pressure distribution due to the unknown experimental pressure distribution, the correction factors, which are defined per panel, are described by a polynomial approach in the spanwise direction and are subject to smoothness constraints in the chordwise direction to prevent arbitrary, non-physical numerical pressure distributions after the model update. The correction factors are then applied to Loads Kernel simulations of dynamic maneuvers to verify their applicability for dynamic cases.

2 AEROELASTIC MODELING

This section describes the structural finite element model and aerodynamic panel model of the TU-Flex FW, as well as the formulation of the pressure and downwash corrections as they are implemented in Nastran and how they are adapted for use in Loads Kernel.

2.1 Finite element model

Figure 3 shows the structural finite element model of the TU-Flex FW. The DLR in-house tool ModGen [15] was used to generate the FE model.

The model consists of 3160 grid points. The wing skin, fuselage section, and spars are modeled using a total of 2140 CQUAD4 quadrilateral shell elements. The foam core of the wing is modeled using 2016 CHEXA solid elements. Servo motors and inertial measurement units (IMUs) are modeled as CONM2 point mass elements connected to the structure with RBE3 elements. The glass fiber laminate used in the wing is modeled by assigning PCOMP properties

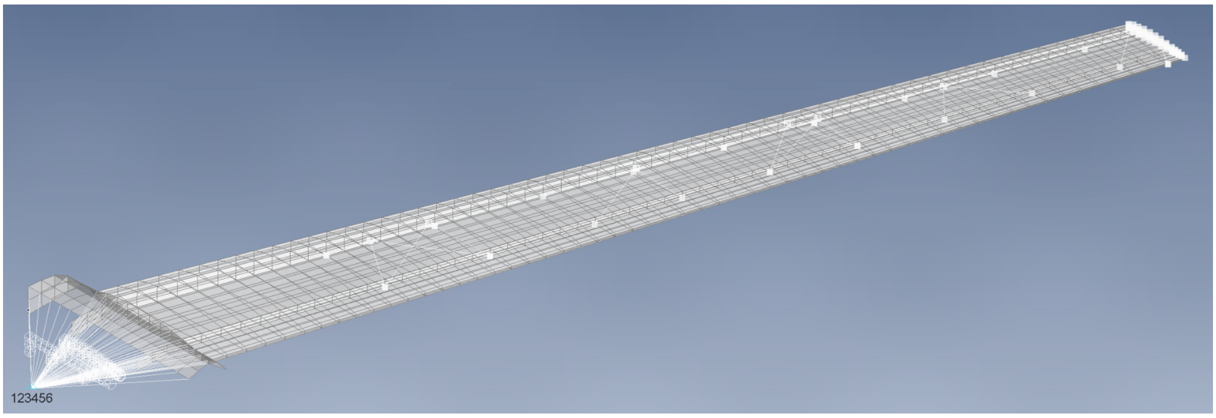

Figure 3: Finite element model of the TU-Flex FW.

to the shell elements, with the individual plies defined using MAT8 orthotropic material cards. The foam core is modeled using MAT1 isotropic material cards. The model is constrained near the wing root by being attached via CBUSH spring elements with a very high stiffness to a node that is clamped in all six degrees of freedom. This node coincides with the load-balance location from the wind tunnel tests. A MONPNT3 monitoring station is defined at this node and gathers the loads, which allows a direct comparison of the loads from simulations and wind tunnel tests.

The structural model of the wing was adjusted using experimental data obtained from static displacement measurements and ground vibration tests to match static deflections, as well as eigenfrequencies and mode shapes [16].

2.2 Aerodynamic panel model

Figure 4 shows the aerodynamic VLM/DLM model of TU-Flex FW. The aerodynamic model contains a total of 708 aerodynamic boxes, of which 672 represent the wing and 36 represent the fairing.

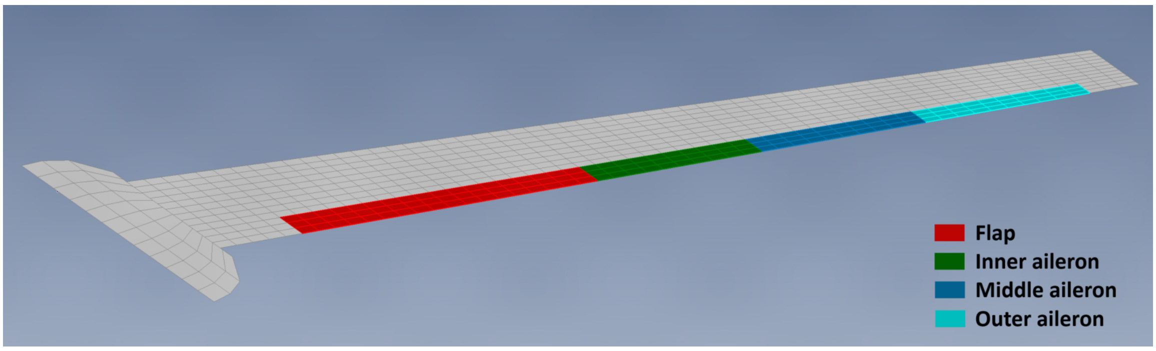

Figure 4: Aerodynamic VLM/DLM model of the TU-Flex FW with boxes making up control surfaces highlighted.

The wing is discretized into 56 spanwise strips and 12 chordwise strips. The spanwise discretization was chosen to correspond to the dimensions of the wing so that the edges of the control surfaces align with box borders. The chordwise discretization of the boxes was chosen so that the aspect ratio of each box is less than three and each box satisfies the condition

$$\Delta x < 0.08V/f \tag{3}$$

with Δx being the chord length of an individual panel, V being the minimum airspeed, and f the maximum frequency of interest [17,18]. The minimum airspeed of the wind tunnel tests was 18 m/s; the maximum frequency of excitation due to maneuvers was 10 Hz during aileron chirps. A maximum frequency of 50 Hz, corresponding roughly to the fourth structural frequency of the wing, was chosen.

2.3 Pressure and downwash correction

Pressure and downwash correction can be implemented in Nastran by using Direct Matrix Input (DMI), i.e., they are explicitly provided by the user. In Nastran, the aerodynamic loads, i.e., the force and moment per box, are calculated as

$$P_k = S_{kj} f_j \tag{4}$$

with P_k being the vector of aerodynamic loads, consisting of alternating entries of box lift and moment, S_{kj} being the diagonal integration matrix that has alternating entries of the area of the box and area times the lever arm between the box midpoint and the box control point on the main diagonal, and f_j being the vector of box pressures, which are calculated from the box downwashes as

$$f_j = \overline{q} A_{jj}^{-1} w_j \tag{5}$$

via the aerodynamic influence coefficient (AIC) matrix A_{jj} and the reference dynamic pressure $\overline{q}$. The downwash on a box is calculated as

$$w_j = [D_{jk}^1 + ikD_{jk}^2]u_k + w_j^g \tag{6}$$

with D_{jk}^1 and D_{jk}^2 being the real and imaginary parts of a differentiation matrix that relates the heave and pitch of a box midpoint in the vector u_k to the resulting downwash w_j at the corresponding box control point. The equation also includes the term w_j^g, which is the additive downwash correction introduced by Giesing et al., and can be interpreted as a vector of user-defined downwashes to account for geometric effects, for example, twist or camber of the airfoil.

The pressure corrections are introduced by expanding equation 4 to

$$P_k = W_{kk} S_{kj} f_j + \overline{q} S_{kj} (\frac{f_j^e}{\overline{q}}). \tag{7}$$

The added terms W_{kk} and $\overline{q} S_{kj}(f_j^e/\overline{q})$ are multiplicative and additive correction factors to adjust the loads on the aerodynamic boxes. W_{kk} is described as "a matrix of empirical correction factors to adjust each theoretical aerodynamic box lift and moment to agree with experimental data for incidence changes" [17]. The W_{kk} correction factors act as multipliers on the pressure of the aerodynamic boxes and, per integration using the S_{kj} matrix on the force and moment, i.e., they change the slope of the lift/moment polar of a box.
$f_j^e/\overline{q}$ is described as a "vector of experimental pressure coefficients at some reference incidence (for example, zero angle of attack) for each aerodynamic element" [17]. The values of this vector are an offset of the pressure coefficient per box, which turns into a force/moment offset via integration. The user provides the values of W_{kk} and $f_j^e/\overline{q}$ via Nastran DMI bulk data entries using the reserved keywords WKK and FA2J. The initial values for an untuned model are ones for W_{kk} and zeros for $f_j^e/\overline{q}$.

3 AEROELASTIC MODEL UPDATING PROCEDURE

In this section, the aeroelastic model updating process is presented. A flow chart of the aeroelastic model updating process is shown below in Fig. 5.

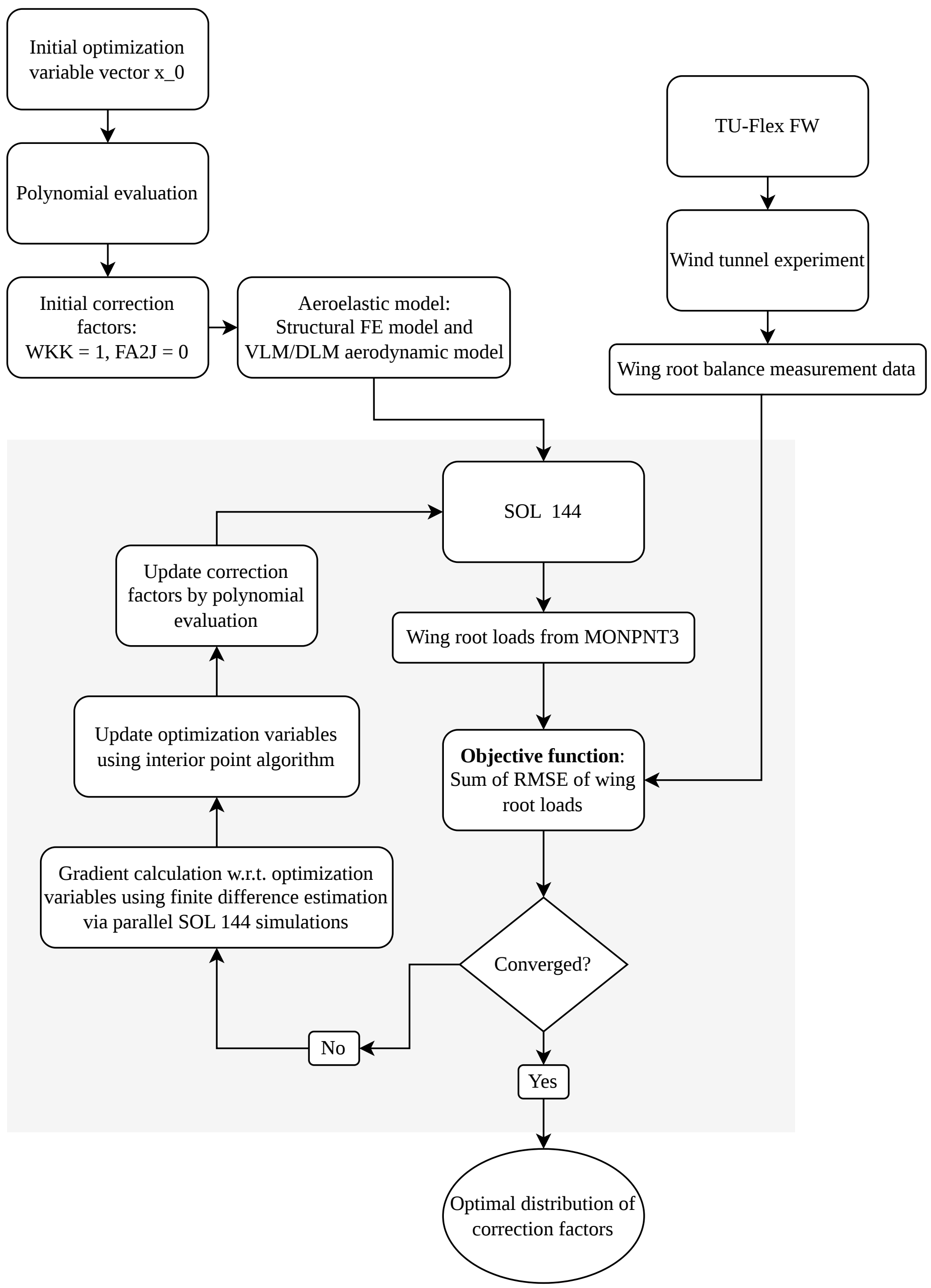

Figure 5: Flow chart of the model updating process.

The optimization routine finds the set of correction factors that minimize the differences in wing root loads acquired from wind tunnel experiments and numerical simulations F_z, M_x, and M_y.

The experimental values were acquired via a load balance; a description of the experimental procedures can be found in [12]. The numerical values for the wing root loads are obtained from a Nastran SOL 144 analysis via a MONPNT3 monitoring station. The objective function to be minimized is defined as the sum of the root mean square errors (RMSE) between simulated and experimental wing root loads at angles of attack of -4, -2, 0, 2, and 4° for a constant airspeed

$$F = \sqrt{\frac{1}{5}\sum_{i=1}^{5}(F^i_{z,sim} - F^i_{z,exp})^2} + \sqrt{\frac{1}{5}\sum_{i=1}^{5}(M^i_{x,sim} - M^i_{x,exp})^2} + \sqrt{\frac{1}{5}\sum_{i=1}^{5}(M^i_{y,sim} - M^i_{y,exp})^2}. \tag{8}$$

In the absence of information about the experimental pressure distribution across the wing, correction factors cannot be determined directly from pressure values. Instead, to ensure a smooth modification of the numerical pressure distribution, the correction factors are assumed to vary spanwise according to a quartic polynomial distribution in each chordwise strip (an illustration is shown in Fig. 6) and are defined as

$$CF(box) = a_4 \cdot y_{norm}(box)^4 + a_3 \cdot y_{norm}(box)^3 + a_2 \cdot y_{norm}(box)^2 + a_1 \cdot y_{norm}(box) + a_0 \tag{9}$$

with a_0 through a_4 being the polynomial factors of the correction factor distribution in a single strip, y being the span location of the boxes, and $y_{norm} := \frac{y}{1.8\text{m}}$.

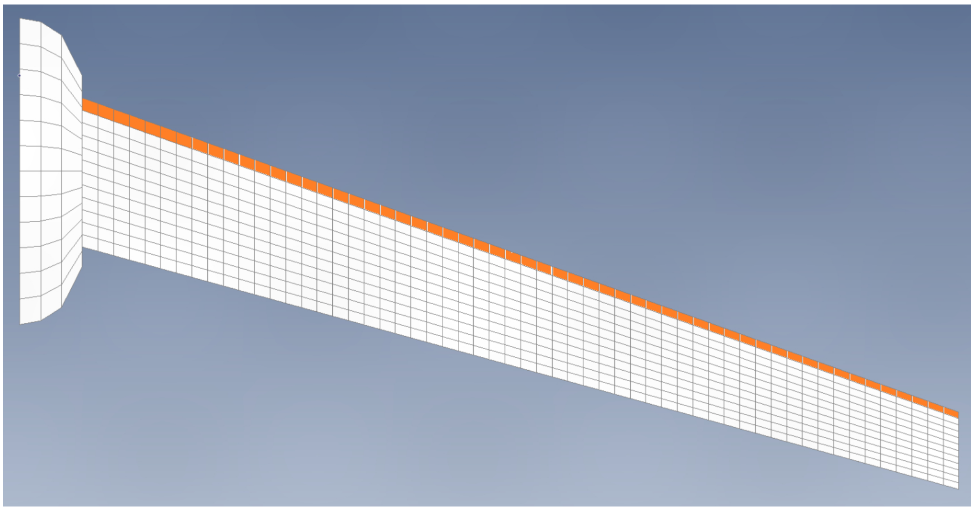

Figure 6: The first strip of aero boxes marked in orange.

To prevent large jumps in the values of chordwise adjacent correction factors, the absolute difference between them is constrained. Three kinds of correction factors are considered: The multiplicative correction factors W_{kk}, which can be conceptually split into a force correction $W_{kk,force}$ and a moment correction $W_{kk,moment}$, and the additive pressure coefficient correction factors $f^e_j/\overline{q}$. The three kinds of correction factors are assumed to be independent of each other. A constant additive downwash correction w^g_j as per equation 6 is defined a priori and corresponds to the camber and twist of the wing.

The optimization routine now consists of finding the combination of values of $W_{kk,force}$, $W_{kk,moment}$ and $f^e_j/\overline{q}$ that minimizes the objective function F. The initial value for all multiplicative correction factors W_{kk} is set to 1; the initial polynomial coefficients are $a_4 = a_3 = a_2 = a_1 = 0$ and $a_0 = 1$. The initial value for the additive correction factors f^e_j is set to 0, and the initial polynomial coefficients are $a_4 = a_3 = a_2 = a_1 = a_0 = 0$. The vector of optimization variables $\mathbf{x}$ is the concatenated row vector of all polynomial factors. With 3*5=15 polynomial coefficients per strip and twelve chordwise strips, this leads to a vector of optimization variables $\mathbf{x}$ of size 1x180 per airspeed. The correction factors are calculated from the optimization variables according to equation 9 and are saved in a 12x56 matrix array, which mirrors the arrangement of the aero boxes. For application in the Nastran simulation, the correction factors are then rearranged into a column vector, with the columns of the 12x56 matrix being stacked on top of each other to follow the convention of numbering the boxes in ascending order in the chordwise direction. The W_{kk} correction factors for force and moment are written to a shared column vector in an alternating fashion. The column vectors are then padded with ones for the W_{kk} and zeros for the f_j^e correction factors, respectively, to accommodate the panels of the fairing near the wing root, which are not included in the optimization.

The correction factors are applied to a SOL 144 simulation by writing the column vectors of correction factors to Nastran .bdf files that contain DMI cards with the reserved keywords WKK and FA2J. Loads Kernel processes box loads using six degrees of freedom per box instead of two like in Nastran. Thus, the correction factors have to be rearranged for use in Loads Kernel simulations by saving them to the appropriate entries depending on the surface normal of the panel.

The optimization procedure of finding the combination of polynomial factors that leads to a distribution of correction factors that minimizes the objective function is performed using the *fmincon* function from the MATLAB Optimization Toolbox. *fmincon* is given the initial values of the optimization variables $\mathbf{x}_0$, the objective function, and the constraints on the differences between chordwise adjacent correction factors formulated in terms of polynomial evaluations of the optimization variables. The objective function is defined as a MATLAB function that gathers the current values of the optimization variables $\mathbf{x}$, calculates the correction factors, writes these to Nastran .bdf files, and runs a Nastran SOL 144 simulation using the correction factors. The wing root loads are gathered from the MONPNT3 output of this simulation, and the value of the objective function is calculated according to equation 8. The objective function is then checked for convergence. If convergence hasn't been reached, the gradient of the objective function with respect to the optimization variables is calculated by performing a finite-difference gradient estimation, in which the current optimization variables are slightly perturbed one at a time, and the resulting change in the objective function is evaluated to approximate the partial derivatives. For 180 optimization variables, this procedure requires 180 SOL 144 simulations per optimization iteration. To increase the speed of the gradient calculation, the 'UseParallel' option is used, which allows multiple finite-difference evaluations to be performed simultaneously.

The correction factors are found independently for five airspeeds of 18, 22, 30, 34, and 40 m/s. For each airspeed, five static load cases of -4, -2, 0, 2, and 4° angle of attack are considered in the optimization.

4 RESULTS

In this section, the resulting correction factors and their impact on the wing root loads for both static and dynamic cases are presented. Figure 7 shows the correction factor distributions that minimized the objective function for all five airspeeds. The force correction factors $W_{kk,force}$ follow a similar distribution for all five airspeeds, with values greater than one near the wing root, peak values of $\sim$1.2-1.3 at the wing root leading edge, and reducing to a value of $\sim$1 at the wing root trailing edge. For all chord locations, $W_{kk,force}$ reduces along the span to values of $\sim$0.35-0.5 at the wing tip, which remain fairly constant over the chord. The distributions for 22 through 40 m/s are very similar to one another, while the distribution for 18 m/s is less smooth across the chord. $W_{kk,moment}$ shows similar behavior for 18 and 22 m/s, starting at a chordwise almost constant value of 0.7 and reducing smoothly along the span to chordwise almost constant values of ~0.2 and ~0.45 at the wing tip, respectively. For the airspeed cases of 30 m/s and above, $W_{kk,moment}$ becomes almost uniform across the wing with values close to 1. f_j^e for 18 m/s has a peak of ~0.6 near the wing root leading edge, decreasing to ~0.25 at the wing root trailing edge. The chordwise distribution remains similar across the span, with a leading edge value of ~0.15 and a trailing edge value of ~-0.2 at the wing tip. For increasing airspeed, the distribution flattens, becoming almost negligible for an airspeed of 40 m/s, with values close to zero across the whole wing.

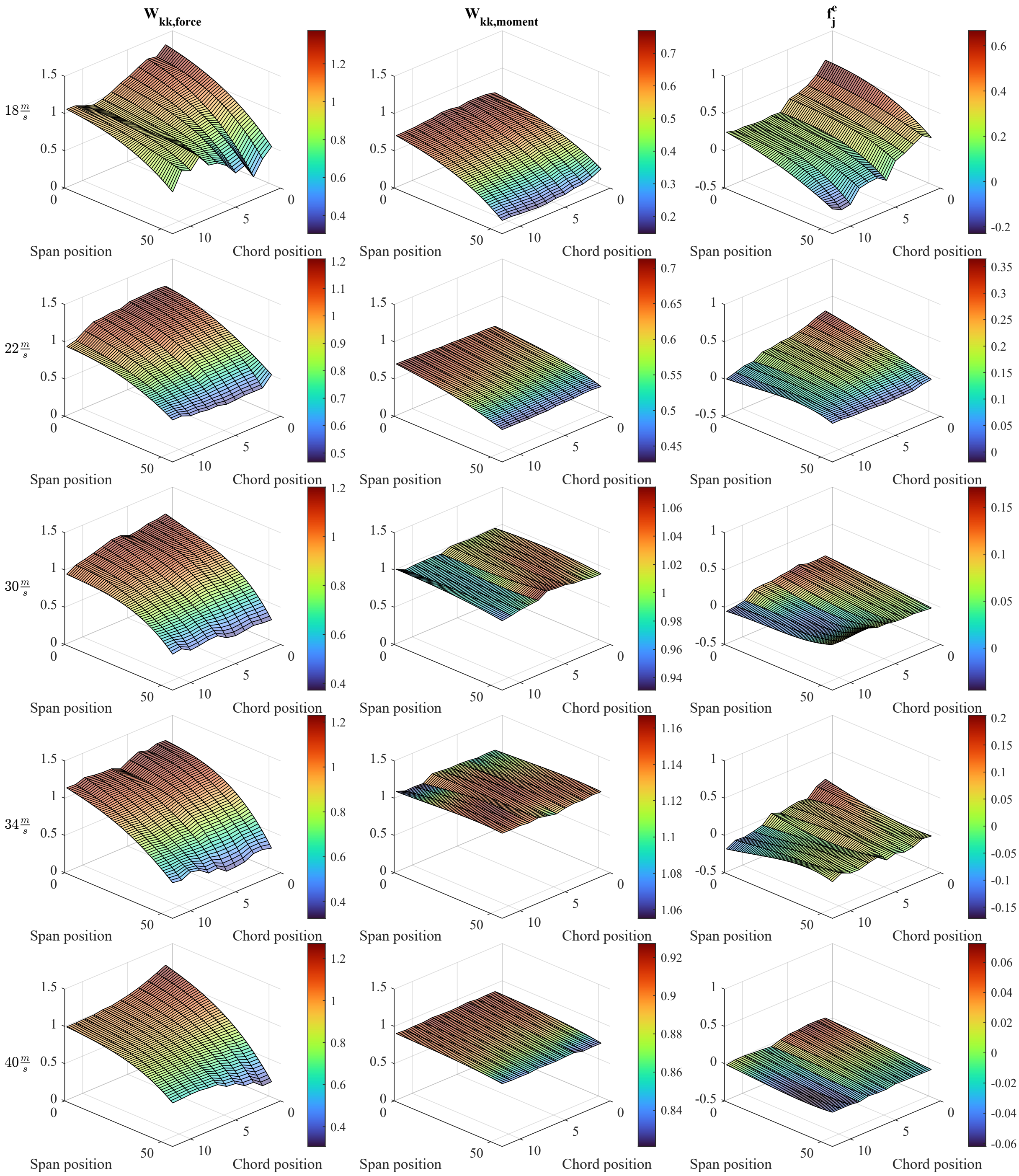

Figure 7: Correction factor distributions for all airspeeds.

4.1 Static cases

Figure 8 compares the wing root loads F_z, M_x, and M_y of the initial and updated model to experimental measurements for angles of attack from -4° to 4° and airspeeds of 18, 22, 30, 34, and 40 m/s. In the initial model, the lift force F_z and bending moment M_x are close to matching the slope for all airspeeds; however, there is a large offset in the 18 and 22 m/s cases, which is eliminated by the correction. For the cases from 30 to 40 m/s, the initial model results already match the experimental measurements quite well in F_z and M_x, but not in M_y. The updated models match the experimental values well for lift, bending moment, and torsion moment. It can be seen that Nastran and Loads Kernel deliver consistent results.

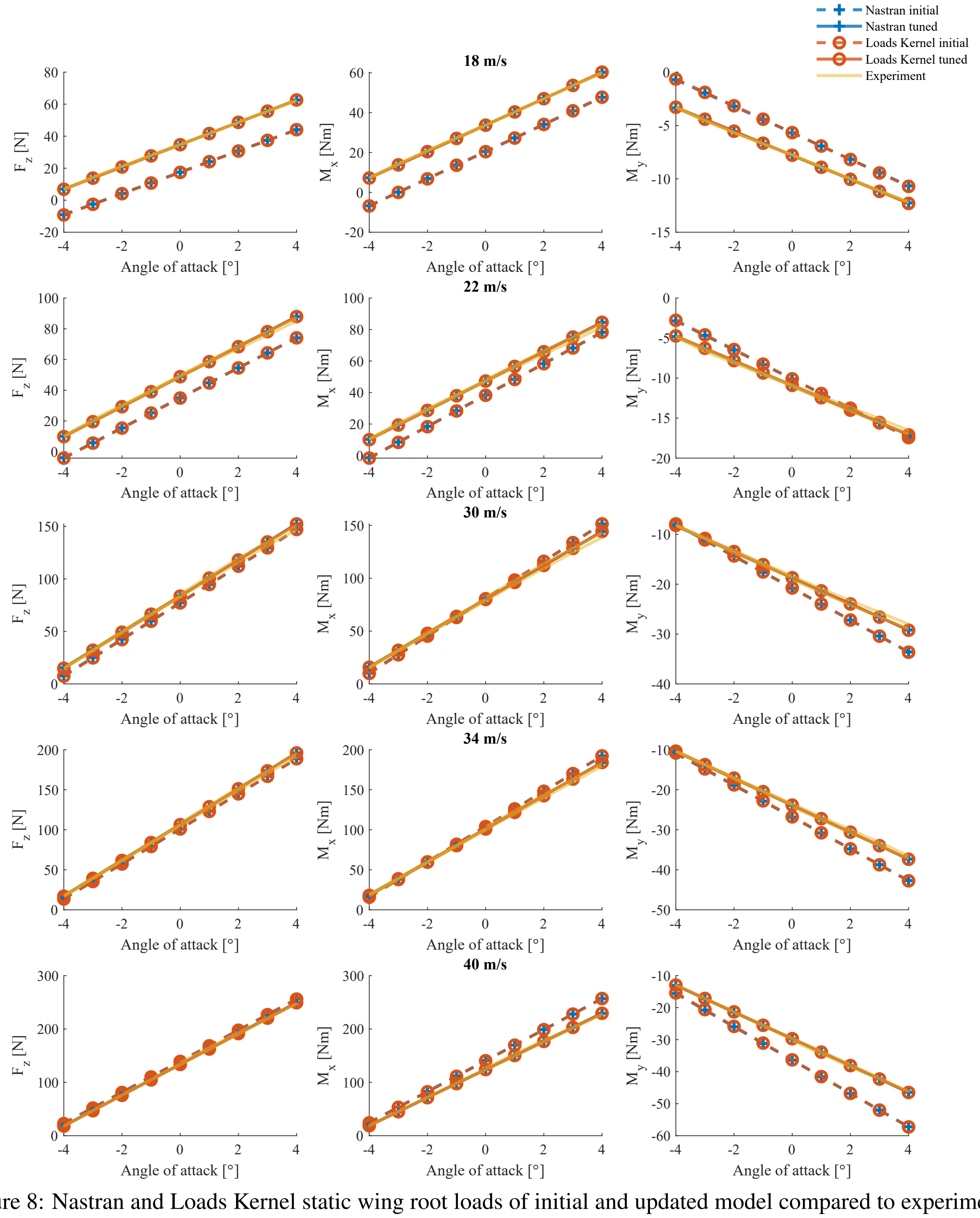

Figure 8: Nastran and Loads Kernel static wing root loads of initial and updated model compared to experimental measurements from -4° to 4° angle of attack.

4.2 Dynamic cases

After validating that the VLM/DLM formulations in Nastran and the Loads Kernel provide consistent results in the static case, dynamic simulations using the correction factors are performed with the Loads Kernel software. In this section, a few sample cases are presented, and the initial and updated models are compared.

4.2.1 Angle of attack variation

Figures 9 through 11 show the wing root loads during dynamic angle-of-attack excitations of different frequencies at a constant airspeed of 30 m/s. The three maneuvers start at initial angles of attack of $\sim$1.3° and increase to $\sim$5° in a 1-cosine shape, with frequencies of 0.5, 2, and 4 Hz relative to the on-flow velocity. These correspond to reduced frequencies of k = 0.0118, 0.0471, and 0.0943, respectively. In the updated model, all three loads are matched in the initial condition for all three cases. The amplitude is slightly underestimated in the updated model compared to the experimental measurements in the 0.5 Hz case, still showing an improvement over the initial model, particularly for the torsion moment. In the 2 Hz case, the amplitude is matched well for all three loads. In the 4 Hz case, the amplitude is matched well for lift and bending moment. The torsion moment measurement shows a higher frequency response and does not follow the angle of attack signal. This can most likely be attributed to an inertial influence of the wind tunnel joiner that connects the wing to the load balance and has significant mass and moments of inertia, which are rotated along with the rest of the wing. The structural model of the wing did not include this wind tunnel joiner and thus cannot account for the associated effects. In the 2 Hz and 4 Hz cases, the loads show an overshoot after the angle of attack returns to its initial value, which is present but not as pronounced in the measurements. Overall, the updated model represents the changes in loads during the dynamic angle of attack variation well. For higher frequencies with significant angle of attack accelerations $\ddot{\alpha}$ the inertia effects of the wind tunnel assembly become relevant, leading to moment responses that are not captured by the model.

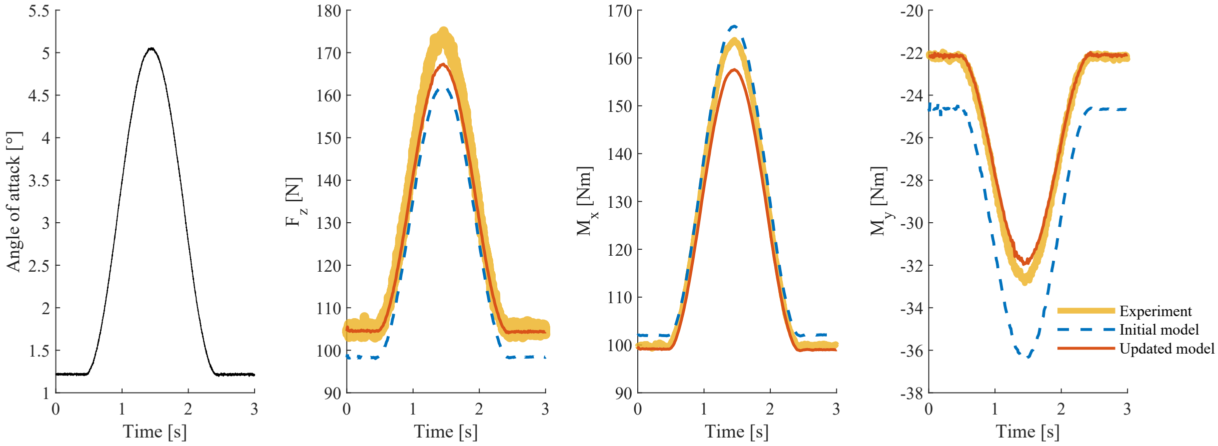

Figure 9: Wing root loads during a dynamic angle of attack variation with a frequency of 0.5 Hz with respect to the on-flow velocity.

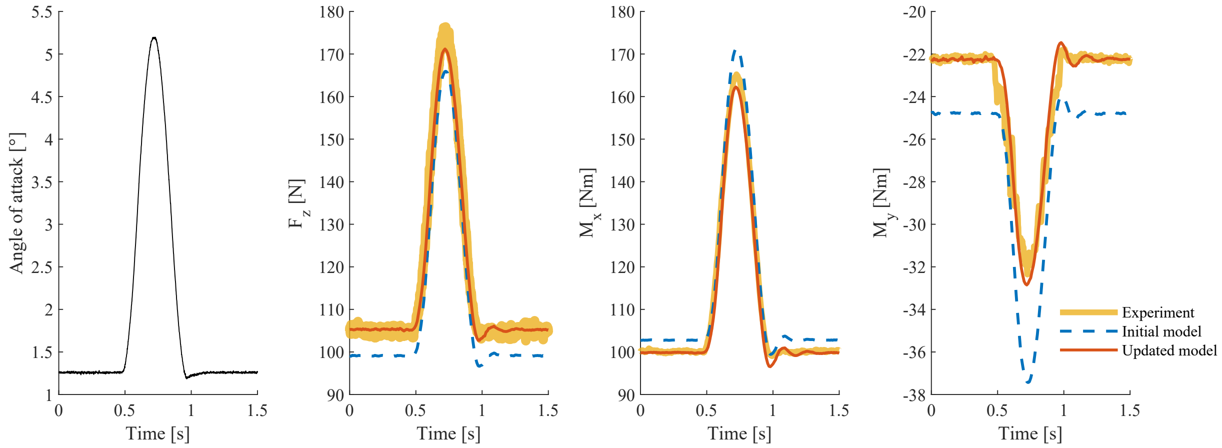

Figure 10: Wing root loads during a dynamic angle of attack variation with a frequency of 2 Hz with respect to the on-flow velocity.

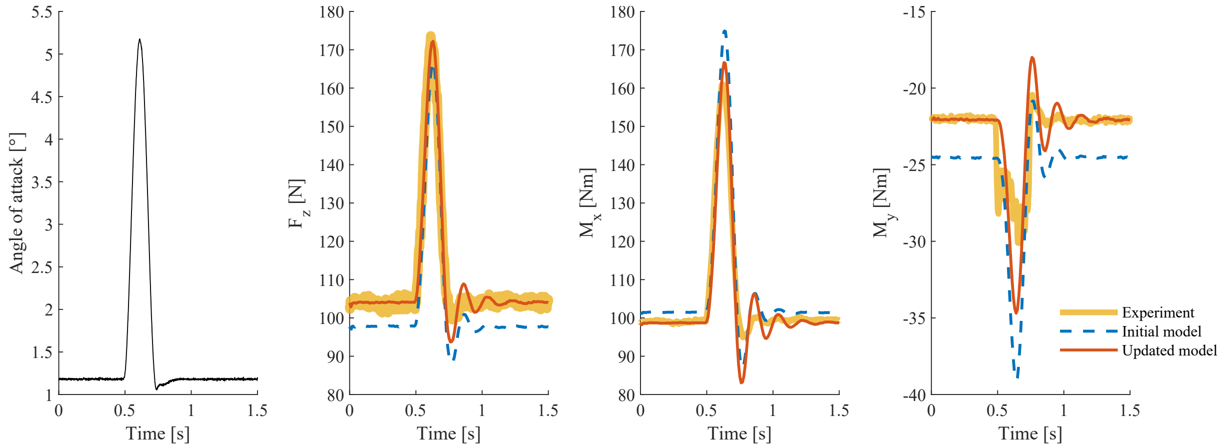

Figure 11: Wing root loads during a dynamic angle of attack variation with a frequency of 4 Hz with respect to the on-flow velocity.

4.2.2 Control surface cases

Doublet maneuvers. Doublet maneuvers are used to validate control surface modeling. Figures 12 through 14 show the wing root loads of the initial and updated models during representative doublet maneuvers of the inner aileron at an airspeed of 30 m/s and an angle of attack of 1.3° for three deflection angles of 5, 15, or 25° compared to experimental measurements.

The updated model matches the experiment well in the loads at the initial trim condition, and the change in loads is modeled well for the 5° deflection case. For 15 and 25° of deflection angle, the model shows larger changes in the loads than those measured in the experiment. The deflection of the control surface induces a linear change in downwash and thus a linear change in the loads. This approximation works well for small deflection angles, but for higher deflection angles, the change in loads gets overestimated. By calculating the ratio of change in loads from the initial trim point between the model and the experiment, an angle correction can be calculated. Figure 15 shows the deflection angles necessary to match the change in loads compared to the input deflection angle for all three ailerons at the four airspeed cases for which experimental data are available. The curves have a sigmoid shape, initially matching the linear reference for a deflection angle of 5° and then departing from the linear reference with increasing deflection angle. This illustrates the nonlinear behavior of the change in loads due to aileron deflection. To include this effect in the aerodynamic model, the input signal for the aileron deflection is modified by premultiplying it with a correction function, which can be calculated from the ratios of the equivalent deflection angle and the input deflection angle. This function is dependent on the airspeed, as the necessary corrections aren't constant for constant aileron deflections at different airspeeds.

$$\delta a = K_{\delta a}(\delta a_{inp}, V) \cdot \delta a_{inp}. \tag{10}$$

This deflection angle correction function is shown in Fig. 16. For the inner and middle aileron, the correction function follows an approximately parabolic trend, remaining close to 1 for small deflection angles and decreasing with increasing deflection. The outer aileron shows a different behavior. Instead of decreasing from values near one for small angles of deflection, the correction factor initially increases sharply, as the necessary deflection angle in the model is higher than the 5° from the experiment. At higher deflection angles, the correction factor decreases. This behavior suggests that the outer aileron correction could be represented by a higher-order polynomial, such as a quartic function. In this work, the corrections are linearly interpolated between the known values. Shown in Fig. 12 through 14 are the results of the aileron doublet maneuver with the modified input signal.

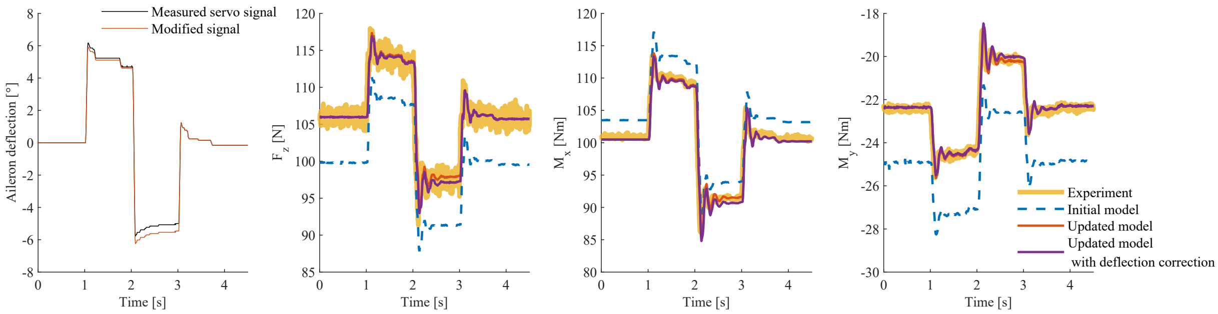

Figure 12: Wing root loads during a 5° doublet maneuver of the inner aileron at an airspeed of 30 m/s.

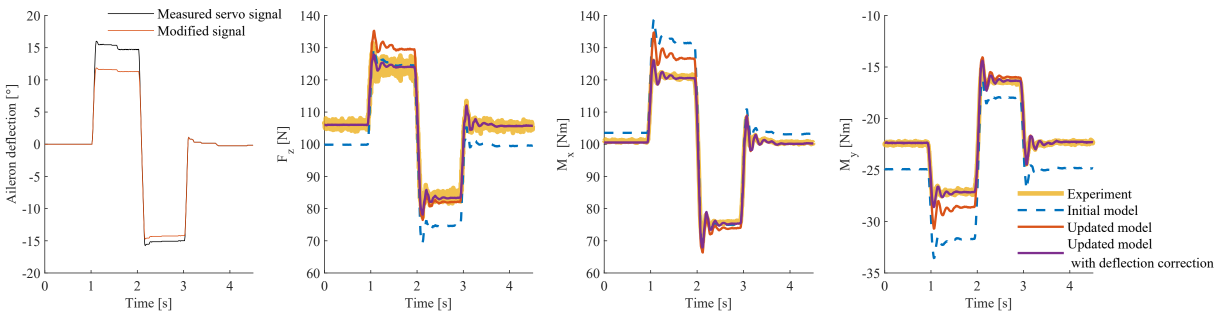

Figure 13: Wing root loads during a 15° doublet maneuver of the inner aileron at an airspeed of 30 m/s.

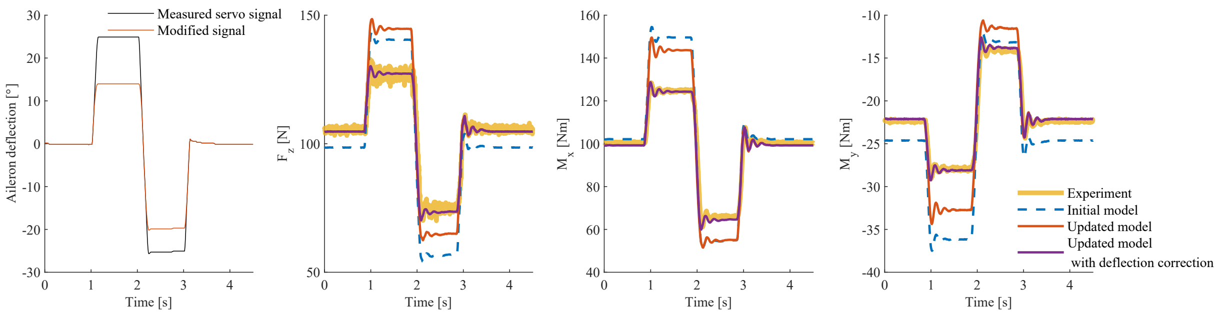

Figure 14: Wing root loads during a 25° doublet maneuver of the inner aileron at an airspeed of 30 m/s.

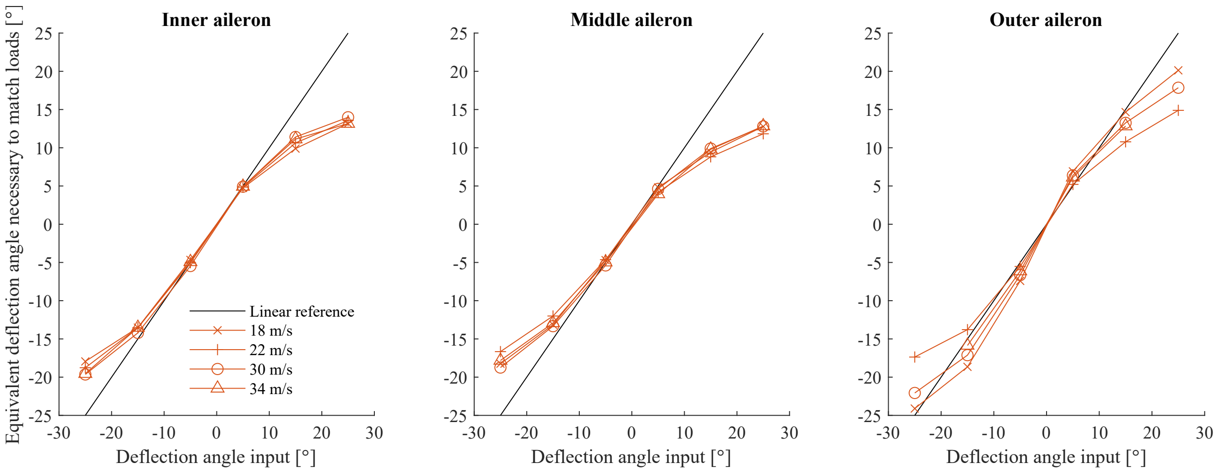

Figure 15: Deflection angles necessary to match the change in loads compared to the input deflection angle for all three ailerons at the four airspeed cases.

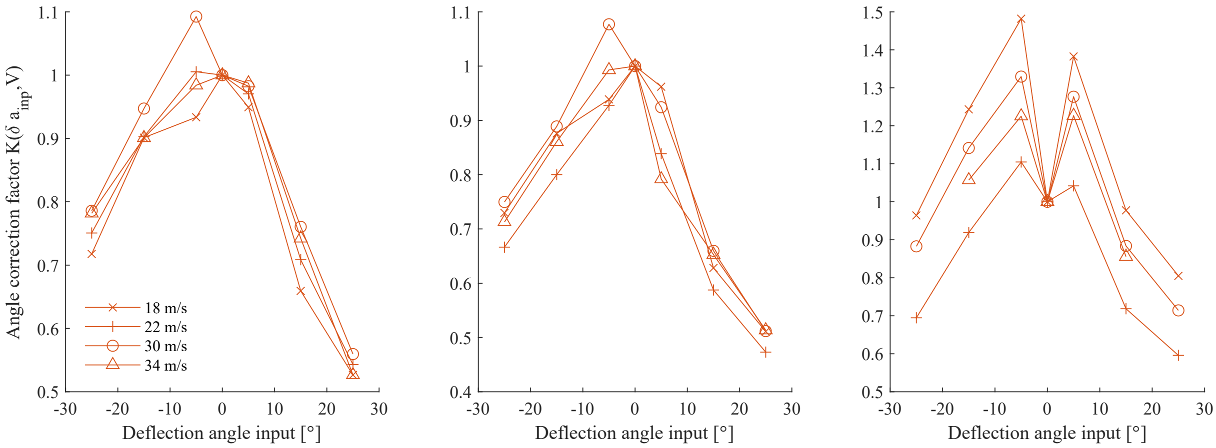

Figure 16: Deflection angle correction functions.

Chirp maneuvers. A series of aileron chirp maneuvers spanning a frequency range of 0 to 10 Hz over a time period of 30 seconds and commanded deflection amplitudes of 2 and 5° were performed for all three ailerons at airspeeds of 18, 22, 30, and 34 m/s. Figure 17 and 18 show the measurements and numerical results of a representative inner aileron chirp maneuver with a commanded amplitude of 5°, at an airspeed of 30 m/s, along with the input signal correction for $\pm 5°$ developed in the previous section. The updated model matched the experimental measurements well in the initial trim condition as well as in the amplitude of the loads. In both the experimental measurements and the model, a noticeable increase in the amplitudes of the loads can be observed near the middle of the time window, coinciding with the chirp frequency approaching the frequency of the first wing bending mode of the wing.

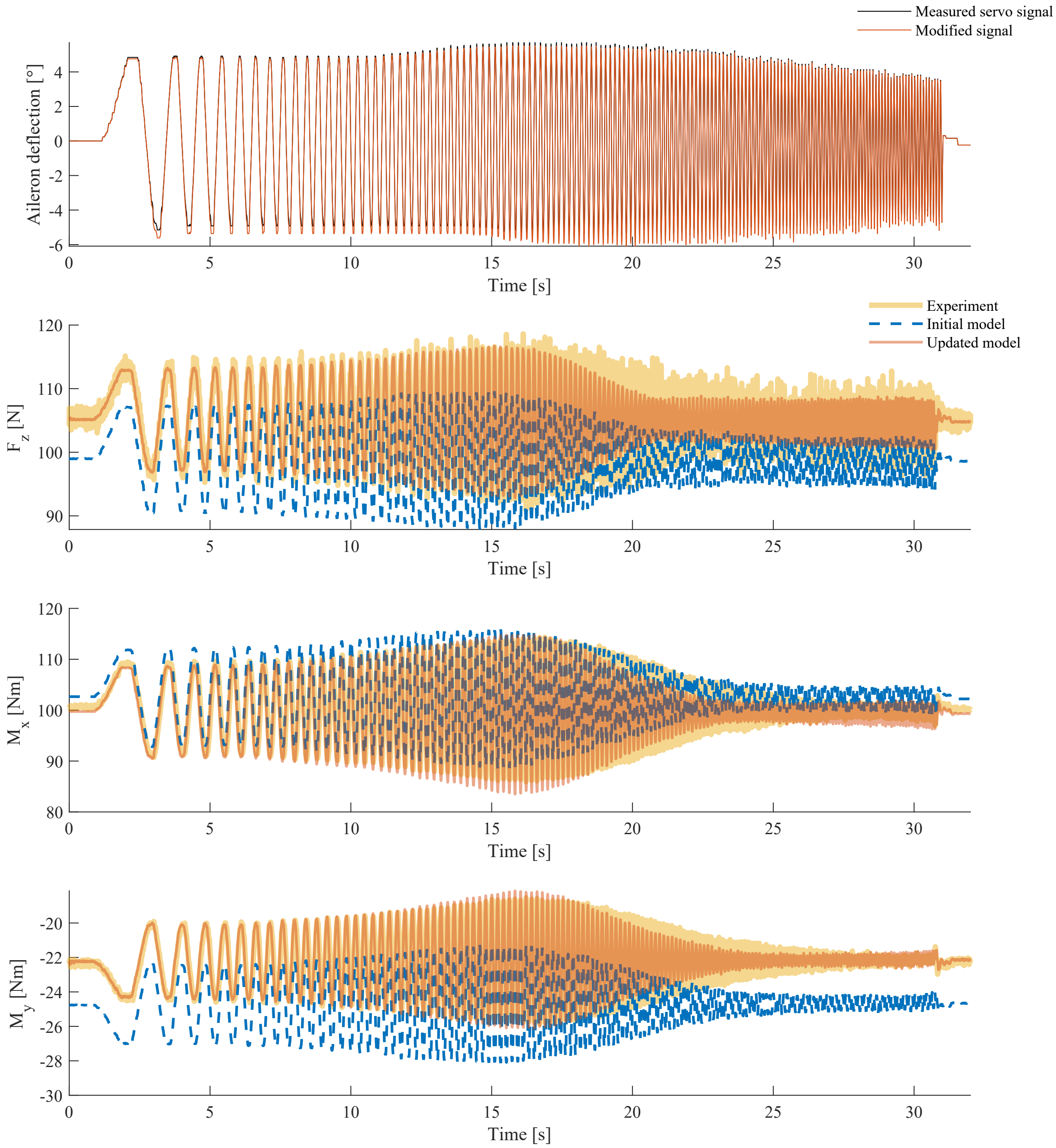

Figure 17: Wing root loads during a 0 to 10 Hz, 5° inner aileron chirp.

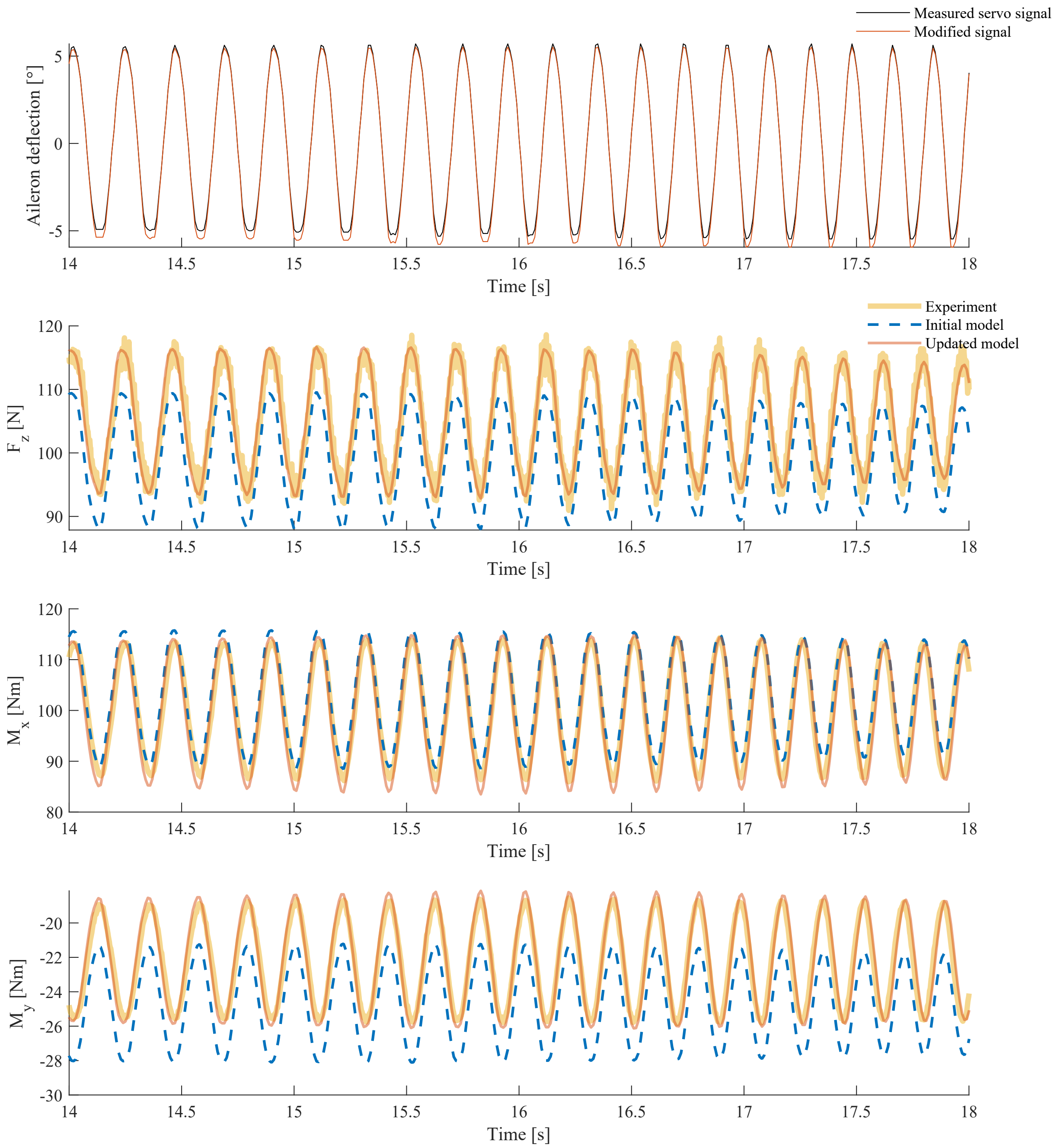

Figure 18: Wing root loads during a 0 to 10 Hz, 5° inner aileron chirp, view focused around resonance with first wing bending.

5 APPLICATION TO FULL AIRCRAFT MODEL & PREVIEW ON FUTURE FLIGHT TESTS

In this section, the correction factors are applied to a model of the full TU-Flex aircraft. The steps for adjusting the correction factors to the full model are explained, and a comparison is made for two static cases and two dynamic maneuver cases simulated using LoadsKernel.

5.1 Modification of correction factor results

Figure 19 shows the aerodynamic model of the full TU-Flex demonstrator. The aerodynamic model consists of a total of 1831 boxes: 1344 of these model the two wings, the vertical stabilizer consists of 135 boxes, and the horizontal stabilizers are modeled by 192 boxes. The fuselage is modeled using a cruciform arrangement of 160 boxes. To apply the correction factors to the whole aircraft model, their spanwise distribution is mirrored to fit the left wing, and the entries are rearranged accordingly. The mirrored correction factor vectors are appended to the original vectors, and the arrays are then padded with ones and zeros, respectively, to accommodate the boxes of the fuselage and tail assembly, for which no correction factors are set.

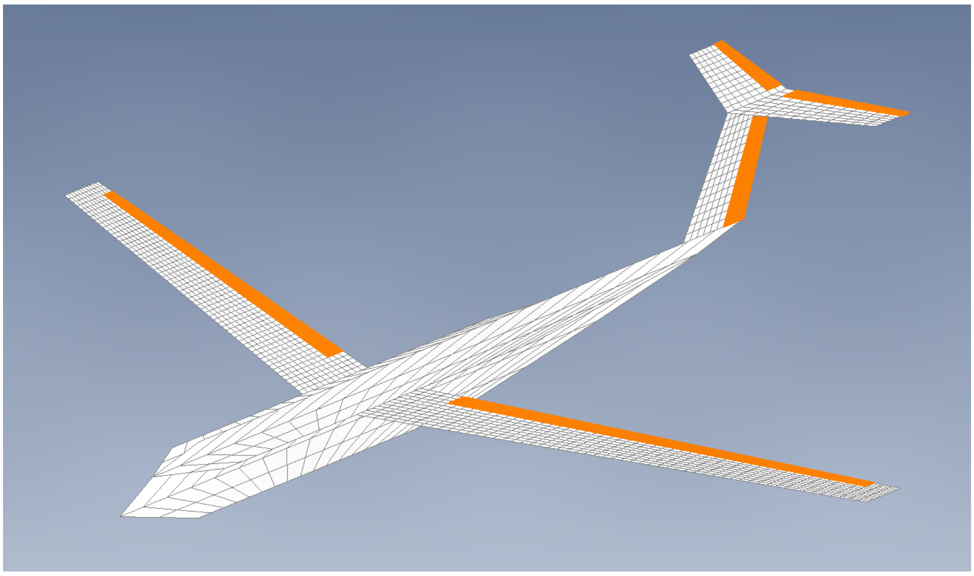

Figure 19: Aerodynamic panel model of the TU-Flex. Control surfaces highlighted.

5.2 Static maneuvers

Two static maneuvers corresponding to corner points of the TU-Flex flight envelope were simulated for both the initial and updated models. These maneuvers, labeled 1 and 2 in Fig. 20, consist of a pull-up maneuver at a pitch rate of 45.56 $^{\circ}/s$ at an airspeed of 37 m/s, corresponding to a load factor of +4, and a push-down maneuver at a pitch rate of -42.16 $^{\circ}/s$ and an airspeed of 42 m/s, corresponding to a load factor of -2. For both maneuvers, the correction factors for the airspeed of 40 m/s were used. Figure 21 shows the resulting deformations during these maneuvers for the initial and updated models. In the updated model, the deflections of the wing during the maneuvers reduce significantly. In the pull-up maneuver, the wing tip deflection reduces from over 0.6 m to $\sim$0.43 m. In the push-down maneuver, the deformation reduces from $\sim$0.3 m downward deflection to $\sim$0.2 m.

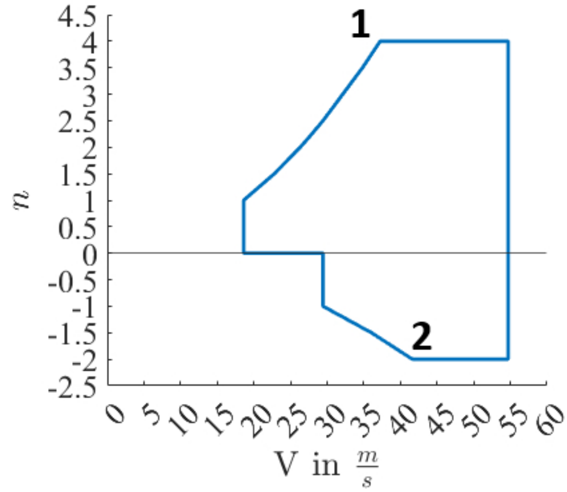

Figure 20: Flight envelope of TU-Flex at sea level with labeled maneuver points.

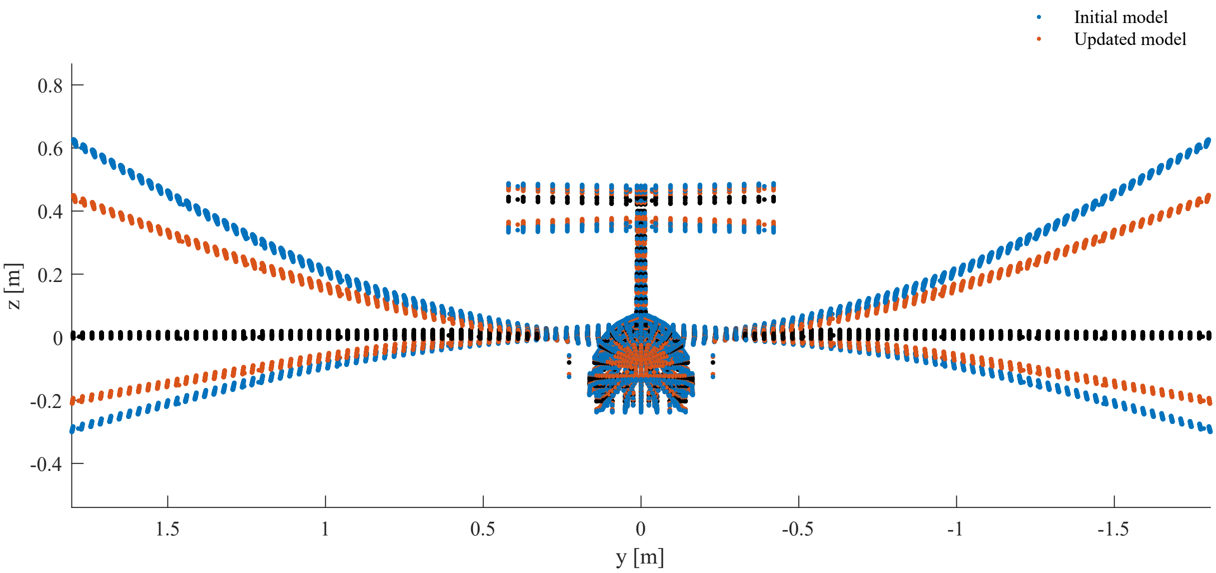

Figure 21: Deformations during pull-up and pitch-down maneuvers of the initial and updated model.

5.3 Dynamic maneuvers

Two representative flight test maneuvers were simulated to compare the initial and updated aircraft models. The first maneuver consists of an asymmetric outer aileron chirp sweeping from 2 to 13 Hz over 8 seconds with an amplitude of $\pm 5°$. The second maneuver is an outer-aileron doublet at a frequency of 5 Hz and an amplitude of $\pm 10°$. Figures 22 and 23 show the results of the simulations, comparing the angle of attack as well as the vertical deflection, acceleration, and angular rates of a node near the right wing tip, which corresponds to the location of an IMU in the wing. The results are qualitatively very similar between the initial and updated models; however, the magnitudes differ. The updated model has an initial trim angle of attack of $\sim 1.87°$ compared to $\sim 2.28°$ in the initial model. Wingtip deformation is reduced in the updated model. During the aileron chirp, both models show an increase in deflection amplitude in the later parts of the chirp, where the chirp frequency approaches the frequency of the second flexible mode. The same behavior can be observed in the accelerations and angular rates of the IMU node. The doublet maneuver shows similar trends. The acceleration and angular-rate responses remain qualitatively consistent between the models; however, their amplitudes are significantly reduced in the updated model

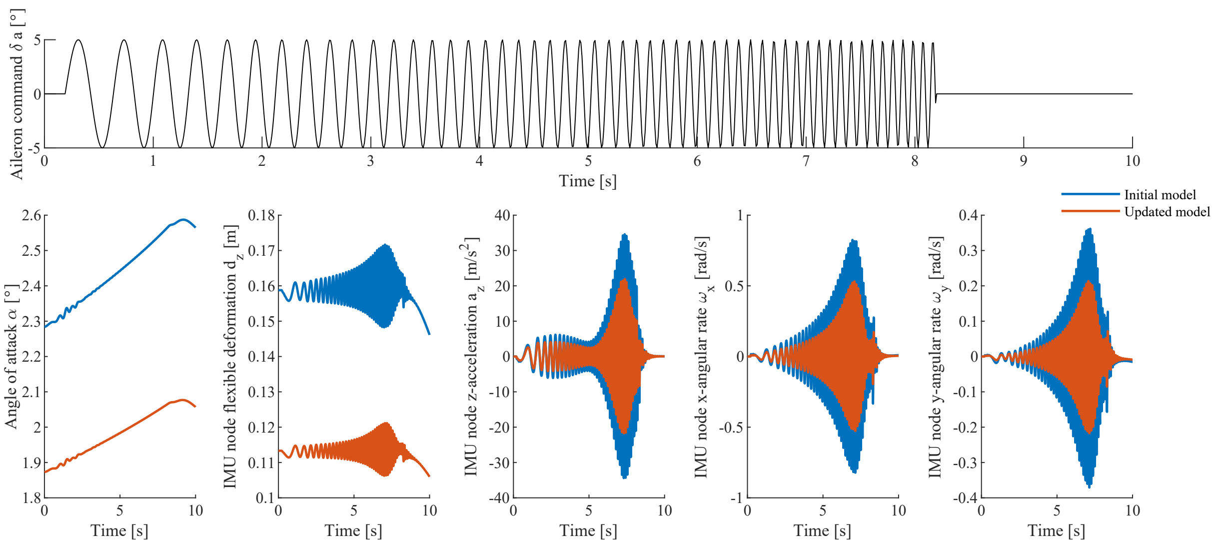

Figure 22: Comparison of initial and updated full aircraft model during an aileron chirp.

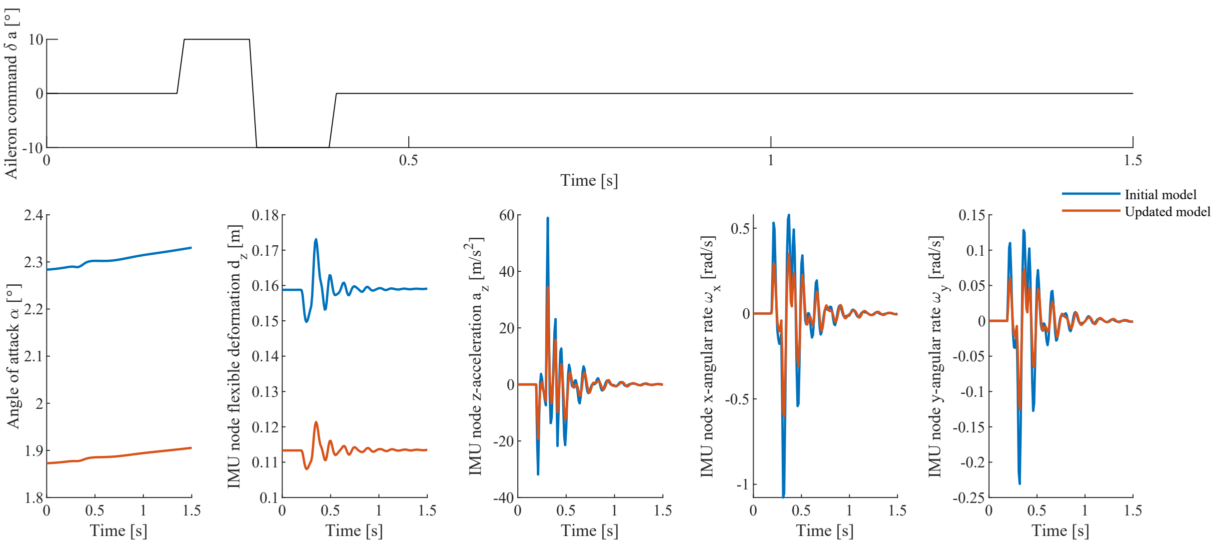

Figure 23: Comparison of initial and updated full aircraft model during an aileron doublet.

6 CONCLUSION & OUTLOOK

This work introduces a methodology for updating aeroelastic VLM/DLM models of wind tunnel models using experimentally measured wing root loads, enabling model calibration without requiring detailed pressure data. Correction factors that minimize the difference between measured and calculated wing root loads are found using an optimization routine and are applied to static and dynamic cases. The updated model demonstrates significantly improved agreement with experimental results for static load cases, as well as good performance in dynamic simulations. Dynamic angle of attack maneuvers are replicated well, with discrepancies likely arising from inertial effects not represented in the structural model. Nonlinear control surface behavior can be incorporated via empirically derived correction functions, which, when applied, lead to a good match with experimental measurements of dynamic control surface maneuvers. The application of the model update results to a model of a full aircraft is demonstrated, and a significant impact on the model results in both static and dynamic cases can be observed, showing the importance of accurate aerodynamic representation for highly flexible configurations.

The proposed method can be expanded by the inclusion of additional measurement data, such as displacement measurements, and by extending the methodology to include frequency-dependent or unsteady aerodynamic corrections to enhance its applicability to higher-frequency dynamic phenomena. The effects of the model update on full aircraft behavior must be further validated, and the approach refined using flight test data.

Overall, the presented method provides a practical framework for aeroelastic model updating using limited experimental data, making it suitable for experimental validation scenarios where detailed pressure measurements or high-fidelity CFD data are unavailable.

ACKNOWLEDGEMENTS

This study was financed in part by the German Federal Ministry for Economic Affairs and Climate Action (BMWK) due to a resolution of the German Federal Parliament within the scope of the LuFo VI-1 project FlexFuture (Grant number 20E2120A).

7 REFERENCES

[1] Palacios, R., Climent, H., Karlsson, A., et al. (2001). Assessment of strategies for correcting linear unsteady aerodynamics using cfd or experimental results.

[2] Giesing, J., Kalman, T., and Rodden, W. (1976). Correction factor techniques for improving aerodynamic prediction methods. Tech. rep., McDonnell Douglas Corporation.

[3] Surampudi, S., Richardson, M., and Dayton, H. (1996). Procedure to match experimental and analytical aerodynamic data for a commercial aircraft. doi:10.2514/6.1996-4191.

[4] Jadic, I., Hartley, D., and Giri, J. (1999). An enhanced correction factor technique for aerodynamic influence coefficient methods.

[5] Moreno, R., von Knoblauch, F., Narisetti, R. K., et al. (2015). A modification to the enhanced correction factor technique to correlate with experimental data.

[6] Mao, K., Jing, W., Cheng, P., et al. (2023). A modification to the enhanced correction factor technique for the subsonic wing–body interference model. *Aerospace*, 10(1). ISSN 2226-4310. doi:10.3390/aerospace10010040.

[7] Utku Gungor, O., Burak Nuzumlalı, A., Ozkesiciler, M., et al. (2024). CFD-corrected aerodynamic influence matrices and applications on aeroelastic phenomena. *J. Phys. Conf. Ser.*, 2647(5), 052004.

[8] Thelen, A. S., Stanford, B., and Jacobson, K. E. (2025). Leveraging a doublet lattice correction method to expedite linearized frequency-domain optimizations in MPhys. American Institute of Aeronautics and Astronautics.

[9] González, P. J., Stavorinus, G., Shahi, H., et al. (2022). A preliminary structural design of a flexible flying demonstrator. In *ICAS 2022 - 33rd Congress of the International Council of the Aeronautical Sciences, Stockholm, Sweden*. ISSN 2958-4647.

[10] González, P., Stavorinus, G., Silvestre, F. J., et al. (2023). *TU-Flex: A Very-Flexible Flying Demonstrator with a Generic Transport Aircraft Configuration*. AIAA SCITECH Forum. doi:10.2514/6.2023-1312.

[11] González, P. J., Shahi, H., Meddaikar, Y. M., et al. (2022). Flexible-wing design process for tu-flex demonstrator. In *IFASD 2022 - International Forum on Aeroelasticity and Structural Dynamics, Madrid, Spain*.

[12] Gonzalez, P. J., Barbosa, G. C., Quesada, A. A. G., et al. (2024). Wind tunnel testing and modal validation of tu-flex's high aspect-ratio wings. In *IFASD 2024 - 20th International Forum on Aeroelasticity and Structural Dynamics, The Hague, Netherlands*.

[13] Voß, A. (2020). Loads kernel user guide. Tech. Rep. DLR-IB-AE-GO-2020-136, German Aerospace Center (DLR). Https://elib.dlr.de/140268/.

[14] Voß, A. (2020). An implementation of the vortex lattice and the doublet lattice method. Tech. Rep. DLR-IB-AE-GO-2020-137, German Aerospace Center (DLR). Https://elib.dlr.de/136536/.

[15] Klimmek, T. (2009). Parameterization of topology and geometry for the multidisciplinary optimization of wing structures. In *CEAS 2009 - European Air and Space Conference*.

[16] Stavorinus, G. (2026). *Structural and Aeroelastic Model Updating Based on Experimental Data*. Master's thesis, Technische Universität Berlin.

[17] MSC Software Corporation, Hexagon AB (2025). *MSC Nastran Aeroelastic Analysis User's Guide*. MSC Software Corporation, Hexagon AB, Irvine, CA, United States.

[18] Rodden, W. P., Taylor, P. F., and Jr., S. C. M. (1998). Further refinement of the subsonic doublet-lattice method. *Journal of Aircraft*, 35(5), 720–727. doi:10.2514/2.2382.

COPYRIGHT STATEMENT